Electronic Supplementary Material (ESI) for Soft Matter

Mechanisms of wetting transitions on patterned surfaces: Continuum and mesoscopic analysis

Michail E. Kavousanakis[1], *Carlos E. Colosqui*[2], *Ioannis G. Kevrekidis,*[2,3] *and Athanasios G. Papathanasiou*[1,*]

[1]School of Chemical Engineering, National Technical University of Athens, 15780, Greece

[2]Department of Chemical and Biological Engineering, Princeton University, Princeton, NJ 08544, USA

[3]Program in Applied and Computational Mathematics, Princeton University, Princeton, NJ 08544, USA

mihkavus@chemeng.ntua.gr (M.E.K.), colosqui@princeton.edu (C.E.C.), yannis@princeton.edu (I.G.K.)

*Author to whom correspondence should be addressed. Tel: +30 210 772 3234, Fax: +30 210 772 3298, email: pathan@chemeng.ntua.gr, web: http://www.chemeng.ntua.gr/people/pathan

Supplementary Information

1. Mesoscopic model for non-ideal fluids and interfacial phenomena

The mesoscopic description based on Eq.(8) employs the BGK ansatz to model the macroscopic effect of short-range fluid-fluid interactions. Non-ideal fluid behavior (e.g. non-ideal equation of state, phase separation) and interfacial effects (e.g. surface tension, disjoining pressure, partial wetting), are modeled by an approximation of the actual force term $\delta f / \delta t = -\mathbf{g}/m \cdot \nabla_{\mathbf{v}} f$ in the kinetic transport equation. Among the different possible approximations[1-3] we adopted the so-called difference method[3] $\delta f / \delta t = f^{eq}(\rho, \mathbf{u}^*) - f^{eq}(\rho, \mathbf{u})$, where the equilibrium distribution is computed using a "shifted" velocity $\mathbf{u}^*=\mathbf{u}+\Delta t\mathbf{g}$.

For the employed class of LB models the volumetric body force $\rho\mathbf{g}$ is obtained as a spatial convolution[4]:

$$\rho\mathbf{g}(\mathbf{x},t) = -\psi(\mathbf{x},t)\int \frac{\mathrm{d}}{\mathrm{d}r} w(|\mathbf{r}|)\psi(\mathbf{x}+\mathbf{r},t)\mathrm{d}r \qquad \text{(SI.1)}$$

of the mean-field pseudo potentials $\psi(\mathbf{x},t)$ with a heuristic kernel w(|r|). It is convenient to adopt a Gaussian kernel $w(|\mathbf{r}|)=(2\pi\kappa\theta)^{-2/D}\exp(-|\mathbf{r}|^2/(2\kappa\theta))$ where the length scale determines the decay of pair correlations due to thermal effects and thus the thickness of the liquid-vapor interface. In all presented results, κ=1.

The volumetric body force $\rho\mathbf{g} = \mathbf{F}_{FF} + \mathbf{F}_{FS}$ thus contains a Fluid-Fluid (FF) component:

$$\mathbf{F}_{FF}(\mathbf{x},t) = \psi_{FF}(\mathbf{x},t)\sum_{i=0}^{Q} w_i \psi_{FF}(\mathbf{x}+\mathbf{r}_i,t)\mathbf{r}_i \ , \qquad \text{(SI.2)}$$

and Fluid-Solid (FS) contribution

$$\mathbf{F}_{FS}(\mathbf{x},t) = \rho(\mathbf{x},t)\sum_{i=0}^{Q} w_i \psi_{FS}(\mathbf{x}+\mathbf{r}_i,t)\mathbf{r}_i \; + \rho(\mathbf{x},t)\phi_S(\mathbf{x})\Delta\mathbf{u}_{wall}(\mathbf{x},t). \qquad \text{(SI.3)}$$

The last term models short-range interactions (i.e. elastic collisions, Pauli repulsion) causing a local shift in fluid velocity $\Delta\mathbf{U}_{wall}=\mathbf{U}_{wall}-\mathbf{u}-\mathbf{F}_{FF}\Delta t$. The wall function $\phi_S(\mathbf{x})$ takes finite values $0\leq \phi_S \leq 1$ vanishing ($\phi_S=0$) at certain distance from the wall. The wall function $\phi_S(\mathbf{x})$ allows an effective control of the slip at the wall as described in[4].

The fluid-solid interactions receive similar treatment to cross-interactions between two components in. The vectors, $\mathbf{r}_i$, and weights, $\mathbf{w}_i$, for the particular lattice employed (D=2 and Q=21)[4] are reported in Table 1.

Table 1: Model Parameters D2Q21

$\mathbf{v}_i,\mathbf{r}_i$[a]	states	w_i
(±1,0),(0, ±1)	1-4	1/12
(±1, ±1)	5-8	2/27
(±2,0),(0, ±2)	9-12	7/360
(±2, ±2)	13-16	1/432
(±3,0),(0, ±3)	17-20	1/1620
(0,0)	21	91/234

[a] lattice units; $\theta=k_BT/m=2/3$

Fluid-Fluid interactions are defined according to:

$$\psi_{FF}(\mathbf{x},t) = \sqrt{2\left[\rho\theta - p_{EoS}(\rho,\theta)\right]}, \qquad \text{(SI.4)}$$

where p_{EoS} is given by the following equation of state (EoS):

$$p_{EoS}(\rho,\theta) = \begin{cases} \rho\theta_V & \text{if } \rho \leq \rho_1 \\ \rho_V\theta_V + (\rho-\rho_1)\theta_M & \text{if } \rho_1 < \rho \leq \rho_2 \\ \rho_V\theta_V + (\rho_2-\rho_1)\theta_M + (\rho-\rho_2)\theta_L & \text{if } \rho > \rho_2 \end{cases}. \qquad \text{(SI.5)}$$

The parameters employed in this work are: θ_V=0.64θ, θ_M=-0.1225θ, θ_L=1.0θ, ρ_V=0.1, ρ_I=0.12823,

ρ_2=0.92096 and ρ_L=1.0. This parameter combination sets two-phase thermodynamic equilibrium at a density ratio ρ_L/ρ_V=10, which results in a compressibility ratio $\beta=\rho_L\theta_L/\rho_V\theta_V$=15.625. Hence, the adopted EoS models a volatile liquid that coexists with significantly less dense (and more compressible) vapor phase while both phases exhibit ideal fluid behavior (i.e. $p \propto \rho$).

A proper choice of the functional form of ψ_{FS} can model a disjoining pressure acting within a distance h from the solid-liquid interface (e.g. h~100nm for many systems of interest). In analogy with DLVO theory, the wall potential $\psi_{FS}(\mathbf{x},t)=G_R\psi_R(\mathbf{x})+G_A\psi_A(\mathbf{x})$ has a repulsive component $G_R\psi_R$ and an attractive component $G_A\psi_A$.

The wall function (ϕ_S) and pseudo-potentials components (ψ_R, ψ_A) are obtained using a recursive Gaussian filter[4]

$$G^{(N_S)}(H(\mathbf{x}))=\sum_{i=1}^{N_S}\sum_{j=0}^{Q}w_j G^{(i-1)}(\mathbf{x}+\mathbf{r}_j\,j,t)\mathbf{r}_j \qquad \text{(SI.6)}$$

that smooths the step function $H(\mathbf{x})$ defining the solid geometry (H=1 within the solid and H=0 in the fluid nodes). For the simulations in this work we use $\psi_R=G^{(5)}(\mathbf{x})$, $\psi_A=G^{(22)}(\mathbf{x})-0.5G^{(5)}(\mathbf{x})$, and $\phi_S=G^{(22)}(\mathbf{x})$.

The repulsive parameter employed in this work is $G_R=\pi/2$ while the attractive parameter G_A takes values within the interval [-1,0]. The static contact angle θ_Y in the present LB simulation is a function of G_A as reported below.

2. Determination of Young's contact angle

The Young's contact angle θ_Y in the LB simulation is determined by the dynamics of fluid-solid and fluid-fluid interactions. Once the EoS and repulsive parameter are fixed, θ_Y becomes a function of the attraction parameter G_A. To obtain the correlation $\theta_Y=\theta_Y(G_A)$, we perform a series of computations for

the equilibrium of a small droplet wetting a planar surface when gravity is ignored.

The liquid/gas interface is considered as the locus of points with a density $\rho=(\rho_L+\rho_G)/2$, where ρ_L and ρ_G the coexistence densities of the liquid and gas phase respectively. We numerically fit a circle to the simulated interface; the contact angle is defined from the slope of the fitting circle at a level (depicted in Figure S1(a) with a black line), beyond which the fluid-solid interactions are of negligible magnitude [4]. The dependence of the computed θ_Y on GA is presented in Figure S1(b).

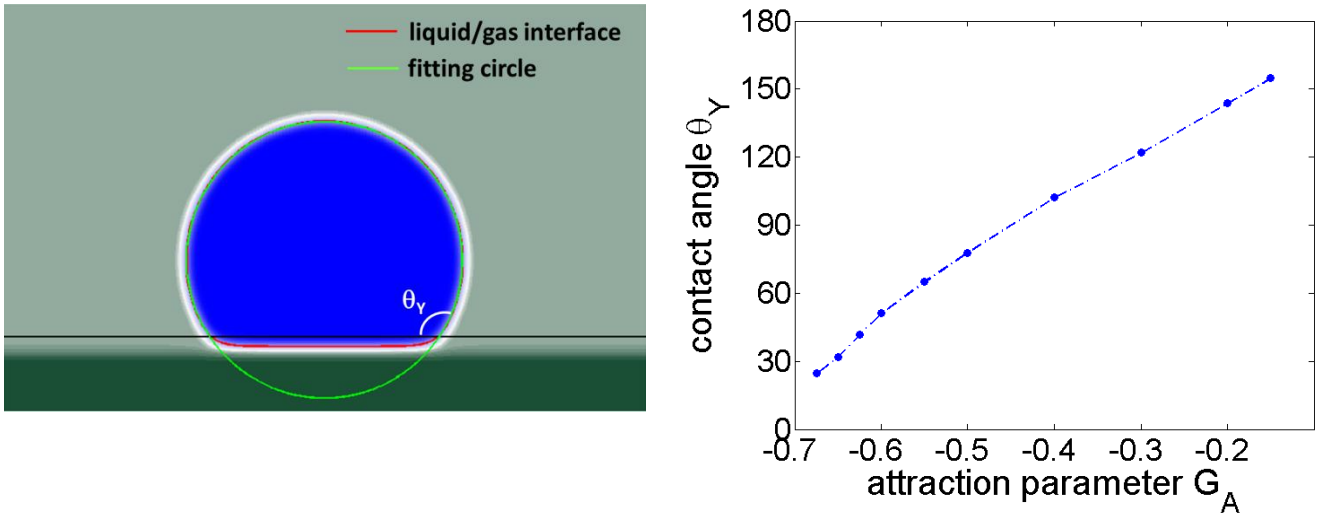

(a) **(b)**

Figure S1. (a) Circular fitting of the liquid/gas interface of a droplet at equilibrium. **(b)** Contact angle (θ_Y) versus attraction parameter (G_A) for a two-dimensional droplet wetting horizontal solid surfaces.

3. Timestepper based GMRES implementation

Depending on the task to be performed (e.g. steady state computation, bifurcation analysis, etc.), different algorithms (e.g. Newton-Raphson, pseudo arc-length continuation) for numerical analysis can estimate 'on demand' the required quantities by performing properly initialized calls to the time-stepper[5-7]. In the case of steady-state computations, the sought solution $\mathbf{U}^*$, satisfies the relation:

$$\mathbf{R} \equiv \mathbf{U}^* - \Phi_T\left(\mathbf{U}^*\right) = \mathbf{0}. \qquad \text{(SI.7)}$$

The solution of (SI.7) is obtained with an iterative Newton-Raphson method in which each iteration step requires the solution of a linearized system

$$\frac{\partial \Phi_T(\mathbf{U})}{\partial \mathbf{U}} \delta\mathbf{U} = -\mathbf{R}(\mathbf{U}) . \tag{SI.8}$$

The guess **U** for the steady-state solution is iteratively updated through $\mathbf{U} \rightarrow \mathbf{U}+\delta\mathbf{U}$ until an adopted convergence criterion is satisfied. The computation of the Jacobian matrix $\frac{\partial \Phi_T(\mathbf{U})}{\partial \mathbf{U}}$ and the residual **R** do not require knowledge of the explicit formulation of the equations to be solved. Their values can be estimated by calling the time-stepper at appropriately perturbed values of the corresponding unknowns. This approach is computationally inefficient for large systems since the estimation of the Jacobian matrix involves the repeated simulation of the time-stepper described by (SI.7) for perturbations in each of the state space directions. Alternatively, one can use matrix-free iterative solvers for the (SI.8) system, e.g. the Generalized Minimal Residual Solver (GMRES)[8, 9], which overcomes this inefficiency given that its algorithmic implementation requires low-cost computation of matrix-vector products $\frac{\partial \Phi_T(\mathbf{U})}{\partial \mathbf{U}}\mathbf{q}$. The set of vectors **q** (**q** is the orthonormal basis of the Krylov subspace, K=span{**b**, **Ab**, $\mathbf{A}^2\mathbf{b}$, $\mathbf{A}^3\mathbf{b}$, ... }, with $\mathbf{A} = \frac{\partial \Phi_T(\mathbf{U})}{\partial \mathbf{U}}$, **b=-R)**, is used to approximate the solution of the linearized system of equations. By calling the time-stepper from nearby initial conditions one estimates the action of the linearized map $\frac{\partial \Phi_T(\mathbf{U})}{\partial \mathbf{U}}$ on known vectors **q**, since:

$$\frac{\partial \Phi_T(\mathbf{U})}{\partial \mathbf{U}}\mathbf{q} \approx \frac{\Phi_T(\mathbf{U}+\varepsilon\mathbf{q}) - \Phi_T(\mathbf{U})}{\varepsilon}, \tag{SI.9}$$

where ε is a small and appropriately chosen scalar (e.g. $\varepsilon = 10^{-7} < \mathbf{U}, \mathbf{q} > / < \mathbf{q}, \mathbf{q} >$ [8]).

4. Timestepper based stability analysis

The stability of a computed steady-state solution, $\mathbf{U}^*$, is determined by solving the linearized eigenvalue problem, $\frac{\partial \Phi_T(\mathbf{U}^*)}{\partial \mathbf{U}^*}\mathbf{u}_{eig} = \sigma\mathbf{u}_{eig}$, where σ is an eigenvalue and $\mathbf{u}_{eig}$ its corresponding

eigenvector. Matrix-free eigensolvers[10] are employed to compute the leading eigenvalues of the Jacobian matrix, $\frac{\partial \Phi_T(\mathbf{U}^*)}{\partial \mathbf{U}^*}$. As in illustration, we present the 20 leading eigenvalues of two wetting states corresponding to a Young angle, θ_Y=110°, in the vicinity of the rightmost turning point C_{LB} (see Figure 3). The solution corresponding to the lower branch is stable with its largest eigenvalue at σ_{max}≈0.91. All the eigenvalues reside within the unit circle on the complex plane and the solution is dynamically stable. On the other hand, the solution on the intermediate branch is unstable, since the largest eigenvalue of the Jacobian matrix is σ_{max}≈1.52.

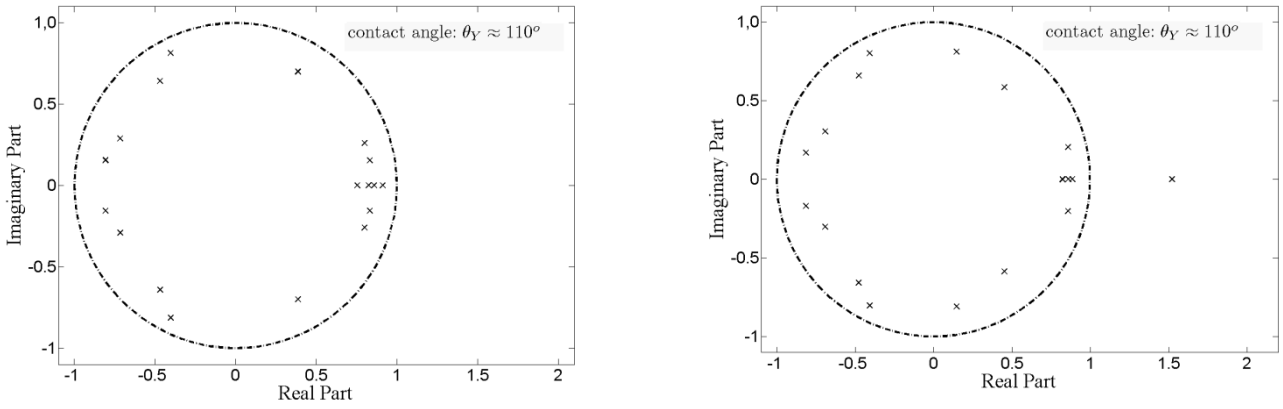

(a) **(b)**

Figure S2. 20 leading eigenvalues of the Jacobian matrix for two wetting states, in the vicinity of the rightmost turning point C. (a) Stable steady-state (branch (III)): all eigenvalues lie within the unit circle on the complex plane. (b) Unstable steady-state (branch (II)): the largest eigenvalue of the Jacobian matrix exceeds unity.

References

1. Benzi, R.; Chibbaro, S.; Succi, S., Mesoscopic Lattice Boltzmann Modeling of Flowing Soft Systems. *Phys. Rev. Lett.* **2009,** 102.
2. Shan, X., Kinetic theory representation of hydrodynamics: a way beyond the Navier–Stokes equation. *J. Fluid Mech.* **2006,** 550, 413-441.
3. Varnik, F.; Gross, M.; Moradi, N.; Zikos, G.; Uhlmann, P.; Müller-Buschbaum, P.; Magerl, D.; Raabe, D.; Steinbach, I.; Stamm, M., Stability and dynamics of droplets on patterned substrates: insights from experiments and lattice Boltzmann simulations. *J. Phys.: Condens. Matter* **2011,** 23, (18), 184112.
4. Colosqui, C. E.; Kavousanakis, M. E.; Papathanasiou, A. G.; Kevrekidis, I. G., Mesoscopic simulation of dynamic wetting phenomena. *Phys. Rev. E*, submitted for publication.
5. Kavousanakis, M. E.; Russo, L.; Siettos, C. I.; Boudouvis, A. G.; Georgiou, G. C., A timestepper approach for the systematic bifurcation and stability analysis of polymer extrusion dynamics. *J. Non-Newtonian Fluid Mech.* **2008,** 151, 59-68.
6. Kevrekidis, I. G.; Gear, C. W.; Hyman, J. M.; Kevrekidis, P. G.; Runborg, O.; Theodoropoulos, C., Equation-free coarse-grained multiscale computation: enabling microscopic simulators to perform system-level tasks. *Commun. Math. Sci.* **2003,** 1, 715-762.
7. Theodoropoulos, C.; Qian, Y. H.; Kevrekidis, I. G., "Coarse" stability and bifurcation analysis using time-steppers: A reaction-diffusion example. *Proc. Natl. Acad. Sci. U.S.A.* **2000,** 97, (18), 9840-9843.
8. Kelley, C. T., *Iterative Methods for Linear and Nonlinear Equations*. SIAM: Philadelphia, 1995.
9. Saad, Y., *Iterative methods for sparse linear systems*. 2nd ed.; SIAM: 1996.
10. Lehoucq, R. B.; Sorensen, D. C., Deflation Techniques for an Implicitly Re-Started Arnoldi Iteration. *SIAM J. Matrix Anal. A.* **1996,** 17, 789-821.